Article
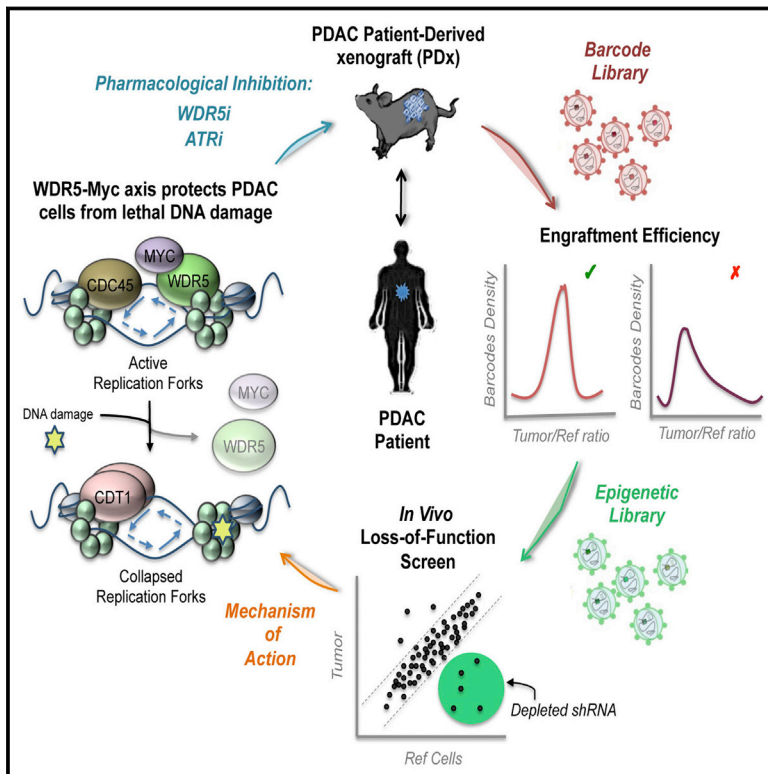
In Vivo Functional Platform Targeting Patient-Derived Xenografts Identifies WDR5-Myc Association as a Critical Determinant of Pancreatic Cancer

Graphical Abstract

Authors

Alessandro Carugo, Giannicola Genovese, Sahil Seth, ..., Luisa Lanfrancone, Timothy Paul Heffernan, Giulio Francesco Draetta

Correspondence

acarugo@mdanderson.org (A.C.),
luisa.lanfrancone@ieo.eu (L.L.),
theffernan@c4therapeutics.com (T.P.H.),
gdraetta@mdanderson.org (G.F.D.)

In Brief

Carugo et al. develop Patient-Based In Vivo Lethality to Optimize Treatment (PILOT), an in vivo and patient-derived xenograft loss-of-function platform, to capture epigenetic vulnerabilities in pancreatic cancer. They report that WDR5-Myc interaction regulates the DNA replication checkpoint illuminating the opportunity to explore WDR5 and ATR inhibitors in the clinical management of pancreatic cancer.

Highlights

- A platform capturing molecular vulnerabilities in patient-derived xenografts is developed

- Rapid engraftment efficiency enables in vivo screens in PDAC

- WDR5-Myc axis protects PDAC cells from lethal DNA damage accumulation

- ATR and WDR5 inhibitors phenocopy the effects of genetic WDR5 suppression

CrossMark

CellPress

Article

In Vivo Functional Platform Targeting Patient-Derived Xenografts Identifies WDR5-Myc Association as a Critical Determinant of Pancreatic Cancer

Alessandro Carugo,[1,4,9,13,*] Giannicola Genovese,[1,4,13] Sahil Seth,[2,13] Luigi Nezi,[1,4] Johnathon Lynn Rose,[1,4] Daniela Bossi,[9] Angelo Cicalese,[9] Parantu Krushnakant Shah,[2] Andrea Viale,[1,4] Piergiorgio Francesco Pettazzoni,[1,4] Kadir Caner Akdemir,[1] Christopher Aaron Bristow,[2] Frederick Scott Robinson,[1,4] James Tepper,[1,4] Nora Sanchez,[1,4] Sonal Gupta,[5] Marcos Roberto Estecio,[6] Virginia Giuliani,[2] Gaetano Ivan Dellino,[9,10] Laura Riva,[11] Wantong Yao,[1,4] Maria Emilia Di Francesco,[1,2] Tessa Green,[1,4] Carolina D'Alesio,[9] Denise Corti,[1,4] Ya'an Kang,[3] Philip Jones,[1,2] Huamin Wang,[7] Jason Bates Fleming,[3] Anirban Maitra,[5] Pier Giuseppe Pelicci,[9,10] Lynda Chin,[1,2] Ronald Anthony DePinho,[8] Luisa Lanfrancone,[9,*] Timothy Paul Heffernan,[12,*] and Giulio Francesco Draetta[1,2,4,*]
[1]Department of Genomic Medicine
[2]Institute for Applied Cancer Science
[3]Department of Surgical Oncology
[4]Department of Molecular and Cellular Oncology
[5]Sheikh Ahmed Bin Zayed Al Nahyan Center for Pancreatic Cancer Research
[6]Department of Epigenetics and Molecular Carcinogenesis
[7]Department of Pathology
[8]Department of Cancer Biology
UT MD Anderson Cancer Center, Houston, TX 77030, USA
[9]Department of Experimental Oncology, European Institute of Oncology, Milan 20139, Italy
[10]Department of Oncology and Hemato-oncology, University of Milan, Milan 20139, Italy
[11]Center for Genomic Science of IIT@SEMM, Istituto Italiano di Tecnologia (IIT), Milan 20139, Italy
[12]C-4 Therapeutics, Cambridge, MA 02142, USA
[13]Co-first author
*Correspondence: acarugo@mdanderson.org (A.C.), luisa.lanfrancone@ieo.eu (L.L.), theffernan@c4therapeutics.com (T.P.H.), gdraetta@mdanderson.org (G.F.D.)
http://dx.doi.org/10.1016/j.celrep.2016.05.063

SUMMARY

Current treatment regimens for pancreatic ductal adenocarcinoma (PDAC) yield poor 5-year survival, emphasizing the critical need to identify druggable targets essential for PDAC maintenance. We developed an unbiased and in vivo target discovery approach to identify molecular vulnerabilities in low-passage and patient-derived PDAC xenografts or genetically engineered mouse model-derived allografts. Focusing on epigenetic regulators, we identified WDR5, a core member of the COMPASS histone H3 Lys4 (H3K4) MLL (1–4) methyltransferase complex, as a top tumor maintenance hit required across multiple human and mouse tumors. Mechanistically, WDR5 functions to sustain proper execution of DNA replication in PDAC cells, as previously suggested by replication stress studies involving MLL1, and c-Myc, also found to interact with WDR5. We indeed demonstrate that interaction with c-Myc is critical for this function. By showing that ATR inhibition mimicked the effects of WDR5 suppression, these data provide rationale to test ATR and WDR5 inhibitors for activity in this disease.

INTRODUCTION

The incidence of pancreatic ductal adenocarcinoma (PDAC) is rising across the world, and the disease is associated with a very high mortality rate: 75% of patients die within the first year of diagnosis and only 7% survive longer than 5 years (American Cancer Society, 2015). The clinical management of PDAC depends on the stage of the disease. Only about 15% of PDAC cases are diagnosed early enough to undergo surgical resection followed by adjuvant therapy (Stathis and Moore, 2010). For patients who are not candidates for surgery, two drugs, gemcitabine and erlotinib, were first approved for PDAC treatment by the US FDA, with two novel regimens approved in recent years, FOLFIRINOX and nab-paclitaxel (Conroy et al., 2011; Von Hoff et al., 2013). However, the impact of chemo-radiotherapy is often transient and produces modest survival benefit.

The majority of pancreatic adenocarcinomas harbor mutant *KRAS*, which plays a key role in reprogramming pancreatic cancer cells into duct-like lineages capable of progressing from pre-neoplastic lesions to advanced PDAC, as demonstrated in genetically engineered mouse models (GEMMs) (Almoguera et al., 1988). PDAC progression is accompanied by genomic deletion and/or loss-of-function mutations in tumor suppressor genes (TSGs), including *TP53*, *CDKN2A*, *SMAD4*, and *PTEN* (Hingorani et al., 2003, 2005). Recent large-scale genome profiling of human PDAC has revealed mutational

events contributing to epigenetic deregulation, as the loss-of-function somatic mutations in three members of the chromatin-modifying COMPASS-like complex family, MLL3, MLL4, and UTX, at a cumulative frequency exceeding 20% of cases (Biankin et al., 2012, Waddell et al., 2015). All COMPASS-like complexes share the core WRAD (WDR5-RBBP5-ASH2L-DPY30) components but assemble selectively with different MLL proteins (MLL1–4), which possess a common H3K4 methyltransferase (MT) activity due to a conserved SET domain, resulting in "activating" marks on chromatin at actively transcribed regions (Trievel and Shilatifard, 2009; Smith et al., 2011). Despite this common function, COMPASS-like complexes have a range of both redundant and non-redundant roles, including methylation-independent roles, in cell development, cell cycle, and differentiation (Smith et al., 2011).

The lack of effective treatment regimens in PDAC has motivated us to conduct a systematic functional approach to target identification, with the goal of identifying druggable epigenetic components. Pooled short hairpin RNA (shRNA) libraries have been exploited to identify in vitro synthetic lethal interactions and targetable genetic dependencies in cancer cell lines (Moffat et al., 2006; Schlabach et al., 2008; Silva et al., 2008; Scholl et al., 2009; Hoffman et al., 2014). Adaptation of these approaches to in vivo screens, predominantly focused on the identification of TSGs in mouse models, expanded our ability to capture more of the cancer biological complexity (Zender et al., 2008; Meacham et al., 2009). Following on recent in vivo screens with human cancer cell lines enforced the importance of capturing the role of key genetic elements in the hallmarks of cancer, including complex heterotypic cancer-host interactions but were limited in their broad application by the inability to efficiently evaluate the xenotransplantation potentials (Possemato et al., 2011; Possik et al., 2014; Baratta et al., 2015). Here, we developed PILOT (Patient-Based In Vivo Lethality to Optimize Treatment), an in vivo platform that enables the identification of oncogenic drivers necessary for tumor maintenance in patient-derived xenografts. This is particularly important given the paucity of novel, and most importantly, truly validated oncology drug discovery targets.

RESULTS

Development of an In Vivo Functional Genomic Screen in Patient-Derived Xenografts

We first established a rapid and reproducible protocol to isolate primary tumor cells from patient-derived xenograft (PDx) tissue or genetically engineered mouse models (GEMMs). These primary models more closely reflect the histologic and phenotypic complexity of human tumors. More importantly, short-term cultures isolated from primary models recapitulate the complex histology of human PDAC (i.e., glandular structures surrounded by dense desmoplasia) when implanted into immunocompromised mice (Figures 1A, S1A, and S1B; Table S1). In vivo shRNA screens rely on the specific elimination of individual shRNAs in a cell population and require therefore that the infected cell population be adequately endowed with tumor engraftment capacity when implanted into recipient mice. The ability of a tumor cell population to engraft and propagate itself when implanted in vivo

varies dramatically among tumor types and must be accurately determined to ensure faithful representation of complex, pooled shRNA libraries (Quintana et al., 2008; Ishizawa et al., 2010). Most commonly, the engraftment efficiency is a measure of the tumor-initiating cell (TIC) frequency, and it is assessed by in vivo transplantation upon extreme limiting dilution assays (Hu and Smyth, 2009; Bonnefoix and Callanan, 2010), but this approach is time consuming and results are widely variable across biological replicates. This limits the use of biologically relevant PDx models, as low-passage human cells have a very low and variable TIC frequency relative to established human and murine cell lines. To rapidly and accurately determine the engraftment efficiency required by each PDAC model, we used a non-targeting "tracking" library expressing 12,500 unique molecular barcodes in early passage tumor samples to "tag" individual cells and assess their fate by comparing clone representation in infected cells with that emerging after tumor establishment in recipient mice (Figure 1B).

To demonstrate the power of the approach, we infected cells isolated from early passage human PDAC xenografts (MDA-PATX43, MDA-PATX50, MDA-PATX53, MDA-PATX66) and PDAC GEMM-derived allografts (*Ptf1a-Cre, Kras$^{G12D\_LSL/+}$, Tp53$^{L/L}$; Ptf1a-Cre, Kras$^{G12D\_LSL/+}$, Cdkn2a$^{L/L}$; Ptf1a-Cre, Kras$^{G12D\_LSL/+}$* escaper line), which displayed either epithelial or mesenchymal histological features (Figure S1B), with the tracking library at a low MOI (less than one integrant/cell) (Figure S1C; Table S2) and implanted infected cells (puromycin selection) subcutaneously into NSG mice. To model optimal library distribution, we analyzed tumors seeded with 80, 240, or 400 individual cells/barcode (Figures 1C, S1D, and S1E). Tumors were isolated from mice, and individual barcodes were quantified by deep sequencing for comparison with the reference cell population. As anticipated, implantation of fewer cells/barcode was required to adequately represent the tracking library (reference/tumor Log$_2$ ratio resulted in a normal distribution) in murine cells (80 cells/barcode) compared to all four PDx cell populations (Figures 1D, S1F, and S1G). We also observed variability among PDx derived samples, demonstrating coverage of the tracking library with implantation of 400 cells/barcode in MDA-PATX53 and MDA-PATX43 (Figures 1E and S1H), but not in MDA-PATX50 and MDA-PATX66 even with implantation of 400 cells/barcode, suggesting the engraftment efficiency in these cell lines was too low to sustain the expression of a library of such complexity (Figures 1F and S1H). Assessment of TIC frequency by extreme limiting dilution was supportive of our conclusions from the tracking library (Figure 1G). Thus, our approach facilitates rapid assessment of xenotransplantation potential in order to optimize experimental design and ensure adequate library complexity, vastly elevating the utility of excised tumor samples for genetic screen approaches.

In Vivo Loss-of-Function Screens to Identify Epigenetic Vulnerabilities in Patient-Derived Xenografts and Mouse Models of PDAC

To explore the utility of our system in the discovery of therapeutic targets, we focused on an extensive collection of chromatin regulators in the context of PDAC. Genetic lesions in chromatin regulators have been identified in a variety of cancers, and new
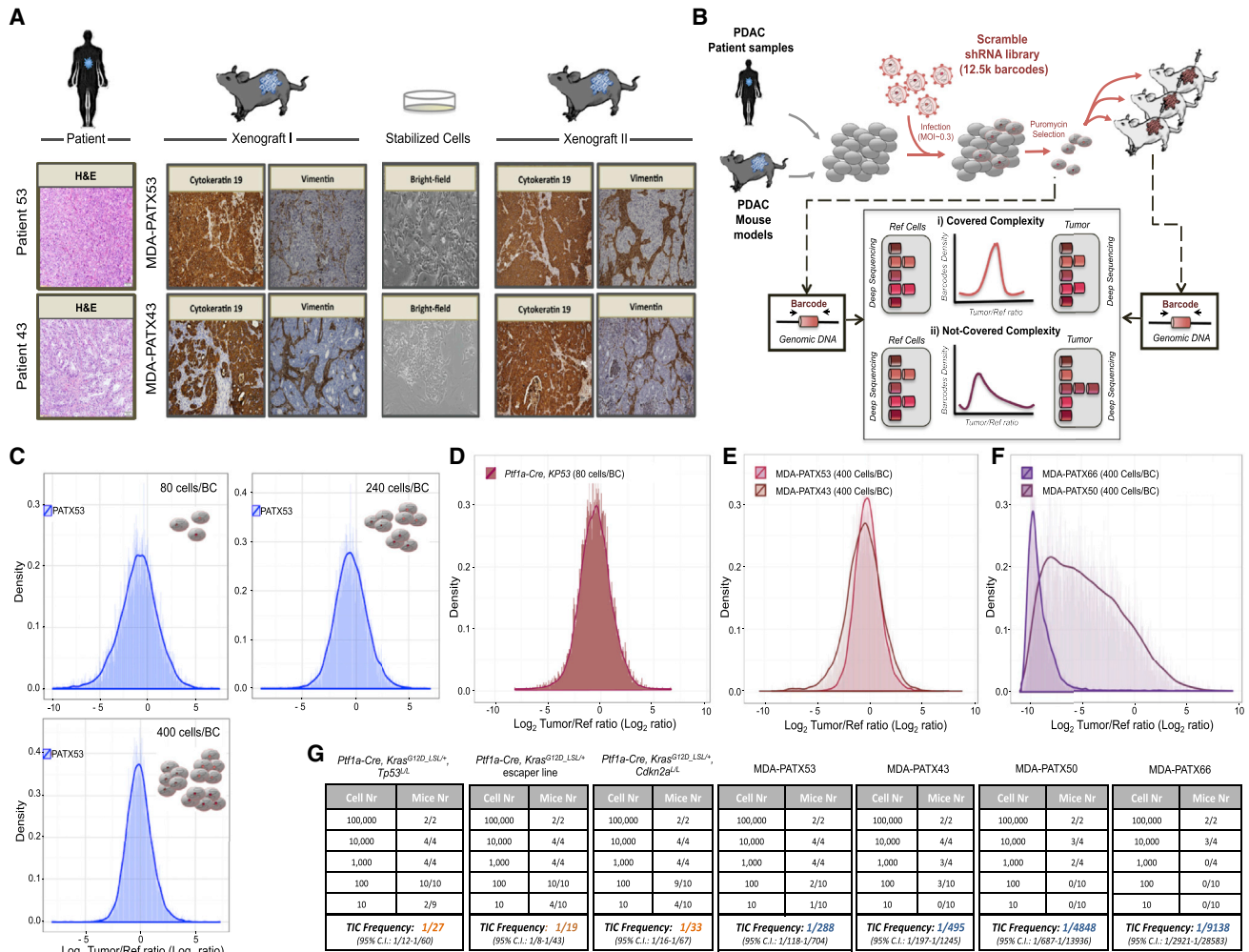
Figure 1. Determination of Engraftment Efficiency Using a Molecular Barcoded-Lentiviral Library

(A) Histological sections of PDAC patients (patient 53, patient 43, 10×) were stained with H&E and compared with the sections collected from the matched PDx models (MDA-PATX53, MDA-PATX43). Xenografts (I–II) were stained for Cytokeratin 19 and Vimentin (10×). Bright field of stabilized cells (20×).

(B) Outline of experimental design for in vivo engraftment efficiency study in xenografts and mouse models of PDAC (MOI; Ref Cells, infected and selected cells before injection; Barcode, 18 unique nucleotides), representative analysis of cells infected with a pool of molecular barcodes (18 nucleotides) (i, model for covered complexity; ii, model for not-covered complexity).

(C) Density plot of the Tumor/Ref Log_2 ratio (median between triplicates) for the xenograft-derived MDA-PATX53 cells infected with the 12.5k barcoded library at increased coverage: 80, 240, and 400 cells/barcode.

(D) Density plot for the Tumor/Ref Log_2 ratio (median between replicates) from the *Ptf1a-Cre, Kras^{G12D_LSL/+}, Tp53^{L/L}* (KP53) cells infected with the 12.5k barcoded library with a coverage of 80 cells/barcode;

(E and F) Density plot of the Tumor/Ref ratio (median between replicates) for the xenograft-derived MDA-PATX43, MDA-PATX50, MDA-PATX53, and MDA-PATX66 cells infected with the 12.5k barcoded library with a coverage of 400 cells/barcode.

(G) Extreme limiting dilution analysis (ELDA) of PDAC GEMM-derived cells and human PDx cells.

See also Figure S1 and Tables S1 and S2.

epigenetic cancer dependencies are emerging as actionable vulnerabilities (Dawson and Kouzarides, 2012; Hoffman et al., 2014). More specifically, epigenetic deregulation is a documented genetic hallmark of PDAC and developmental oncobiology overall, implying a causal role in disease pathogenesis (Omura and Goggins, 2009). To probe epigenetic vulnerabilities in PDAC, and guided by the engraftment efficiency results from our tracking library, we enlisted three murine cell lines and MDA-PATX53 and MDA-PATX43 in in vivo screens of an shRNA library targeting 236 unique mouse or human epigenetic regulators (Figures 2A, S2A, and S2B). To enhance the robustness of the screen and facilitate hit prioritization, the library was designed with ten unique shRNAs targeting each epigene. To ensure adequate representation of the complexity of our deep-coverage epigenetics library in human and mouse samples, mice were implanted respectively with 2,000 cells/shRNA and 400 cells/shRNA, and barcode abundance was quantified in established xenografts by deep sequencing (Figures 2B, 2C, S2C,
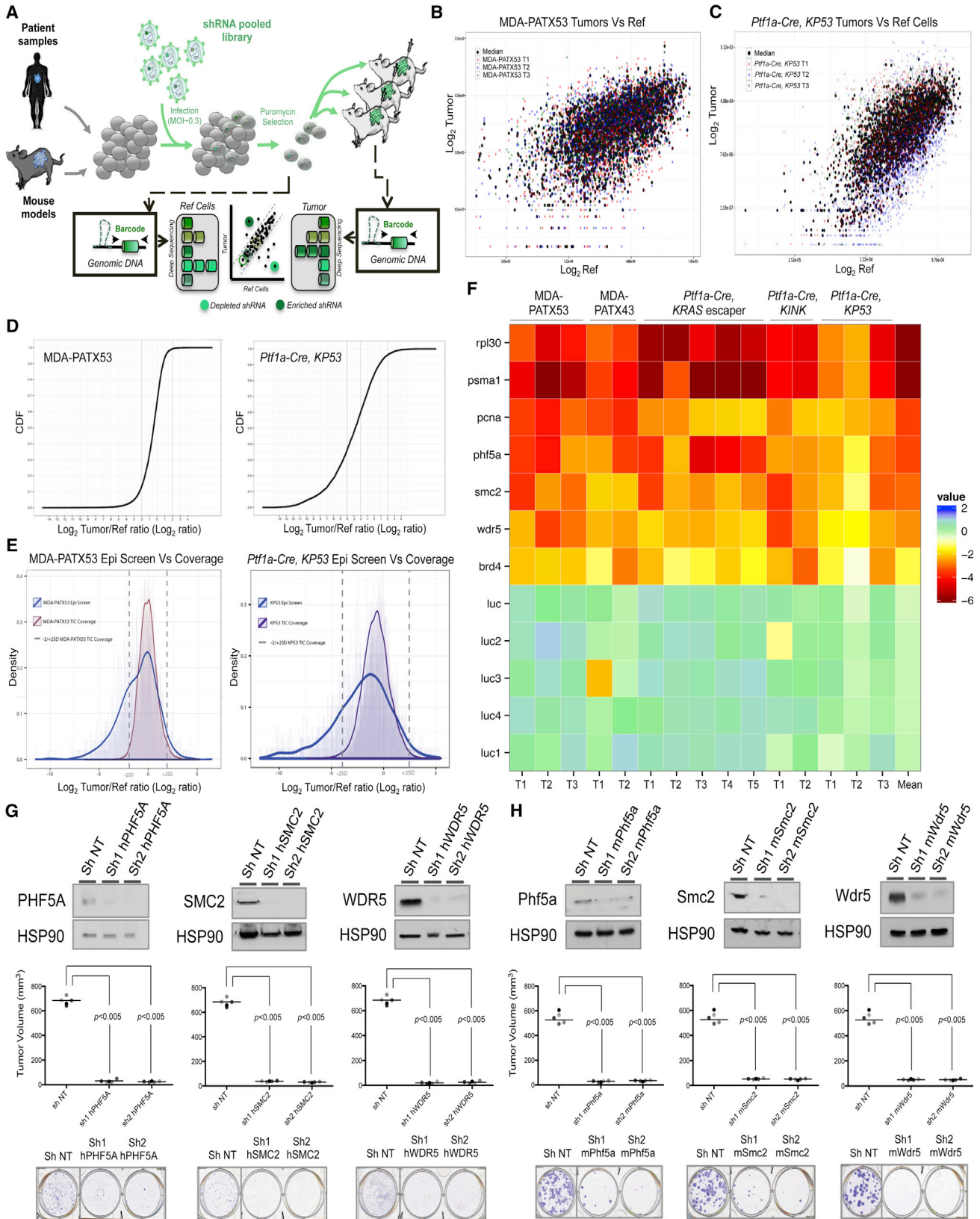
(legend on next page)

and S2D). Comparison among replicates (Pearson's correlation factor) confirmed the usefulness of our tracking approach in predicting the engraftment efficiency (Figure S2E).

To detect the top 15%–30% most-depleted shRNAs we applied a cumulative distribution function (CDF) as a first-line filter, using thresholds of $-2/-4$ Log_2 (Figure 2D). Imposing the same thresholds on the previously introduced engraftment efficiency study with the tracking library (see above), we observed less than 2.5% barcode scoring, substantiating that we were only detecting significantly depleted hairpins (Figure 2E). Multiple methods were leveraged to evaluate "hits" (or top-scoring genes) emerging from our screens, including mean of the top-scoring three hairpins and p values from RSA (or redundant shRNA activity) scores (Figure 2F). Notably, irrespective of the used approach, two well-known essential genes encoding for a proteasome (*PSMA1*) and a ribosomal (*RLP30*) protein added to the library as positive controls scored among the most-depleted hits (Figure 2F), as did *PHF5A*, *SMC2*, and *BRD4*, all known to have a role in cancer (Hubert et al., 2013; Krattenmacher et al., 2014; Sahai et al., 2014). Unsupervised clustering analysis of all genes in the library validated replicates across tumors but also identified vulnerabilities unique to each model (Figure S3). Downregulation of PHF5A, SMC2, and WDR5 using two independent singleton shRNAs significantly impaired new colony formation and tumor growth in both human (Figure 2G) and mouse PDAC models (Figures 2H and S2F).

WDR5 Is Essential for PDAC Initiation and Proliferation

One of the most robust hits to emerge across multiple screens was the WD repeat-containing protein 5 (*WDR5*), a core member of the COMPASS histone H3 Lys4 (H3K4) methyltransferase complex (Steward et al., 2006; Trievel and Shilatifard, 2009; Smith et al., 2011). Recently, WDR5 upregulation was detected in prostate and bladder cancers, where it was also found to be critical for cancer cell proliferation (Kim et al., 2014; Chen et al., 2015). We first confirmed deregulated expression of WDR5 in human PDAC compared to normal control pancreas (Figure 3A). WDR5 knockdown dramatically affected tumor growth of orthotopically implanted patient-derived PDAC cells and extended survival compared to non-targeting (NT) shRNA controls (Figure 3B). The observed effects were confirmed to be on target, as expression of ectopic *WDR5* cDNA lacking the 3′ UTR targeted by the shRNA rescued the impairment in colony formation ability upon WDR5 knockdown (Figures 3C and S4A). Next, we confirmed an essential role across multiple primary patient-derived PDAC in vivo models (Figures 3D and S4B). Moreover, we also generated pancreatic cancer spheres from both human and mouse PDAC samples using serum-free 3D growth conditions (Viale et al., 2014). Consistent with the observed in vivo response, WDR5 knockdown significantly impaired the spherogenic potential of these tumor-initiating cells, as demonstrated by calcein staining and spheroid counts (Figures S4C and S4D).

To evaluate whether WDR5 was essential for proliferation of an established PDAC tumor, we infected patient-derived cells (MDA-PATX53 and MDA-PATX66) with Tet-inducible WDR5 shRNA (Sh1 hWDR5i, Sh2 hWDR5i) or control shRNA constructs (Sh NTi) and transplanted them in host mice (n = 5) (Figure S4E). We observed a dramatic growth arrest of established tumors upon WDR5 downregulation under doxycycline treatment that was maintained through the end of the study (Student's t test, $p < 0.05$) (Figures 3E, 3F, and S4F). Immunohistochemistry staining confirmed that WDR5 knockdown was positively correlated with a robust reduction of the proliferation marker Ki67 (Figure 3G). Taken together, these data confirm that WDR5 is a critical regulator of tumor growth in human PDAC.

WDR5 Inhibition Arrests Tumor Progression of Autochthonous PDAC Models

To further validate the biological role of WDR5 in tumor maintenance, we developed an autochthonous lentiviral-based somatic-mosaic (pLSM5) in vivo system. We designed a modular system by combining the Cre-LoxP and Flpo-Frt technologies in a single vector, thereby generating PDAC cells carrying a latent shRNA to allow time-restricted, acute inactivation of any gene of interest in established tumors generated from cells transplanted in the pancreas of host recipients (Figure 4A). Specifically, early epithelial progenitor cultures were established from $R26^{Cag-FlpoERT2/+}$; $KRas^{G12D\_LSL/+}$; $Tp53^{L/L}$ or $Rosa26^{mTmG/+}$ embryonic livers and expanded ex vivo (Zender et al., 2008). Cells were transduced with the pLSM5 system where a Frt-stop-Frt cassette containing the Cre recombinase under the *Krt19* promoter was cloned between the U6 promoter and the shRNA and transplanted in immunocompromised $Rag2^{-/-}$ mice pretreated with cerulein (Figure S5A). Specifically,

---

Figure 2. In Vivo shRNA Screens of Epigenetic Vulnerabilities in Patient-Derived and Mouse Models of PDAC

(A) Outline of experimental design for deep-coverage shRNA screens in xenografts and mouse models of PDAC (MOI; Ref Cells, infected and selected cells before injection; Barcode, 18 unique nucleotides).

(B) MDA-PATX53 cells were screened in triplicate with a coverage of 2,000 cells/shRNA (Tumor/Ref Log_2 ratio).

(C) *Ptf1a-Cre, Kras$^{G12D\_LSL/+}$, Tp53$^{L/L}$* (KP53) cells were screened in triplicate with a coverage of 400 cells/shRNA (Tumor/Ref Log_2 ratio).

(D) Cumulative distribution function (CDF) of shRNA's fold change (Tumor/Ref Log_2 ratio) for human MDA-PATX53 (left panel) and *Ptf1a-Cre, Kras$^{G12D\_LSL/+}$, Tp53$^{L/L}$* (KP53) mouse model (right panel).

(E) Overlapped Tumor/Ref ratios (Log_2 ratio) of the engraftment efficiency studies and the corresponding shRNA screens in MDA-PATX53 (left panel) and *Ptf1a-Cre, Kras$^{G12D\_LSL/+}$, Tp53$^{L/L}$* (KP53) (right panel), Log_2 ratio values corresponding to the ±2 SDs in the engraftment coverage (TIC) studies are highlighted in the graphs (dashed gray lines).

(F) Heatmap of the top-scoring hits generated applying a p value-based cutoff ($p < 0.05$) associated with the Z score (fold change, average of the top three shRNAs), Ranking determined applying the mean Z score. Negative controls (Luc1–4), positive controls (Psma1, Rpl30, Pcna).

(G and H) Western blot, xenotransplantation tumor size (mm^3) and colony formation assay for the human MDA-PATX53 and mouse *Ptf1a-Cre, Kras$^{G12D\_LSL/+}$, Tp53$^{L/L}$* (KP53) cells infected with two independent shRNAs against the top-scoring hits: WDR5, PHF5A, and SMC2 (h, human; m, mouse). Data are mean ± SD. See also Figures S2 and S3.
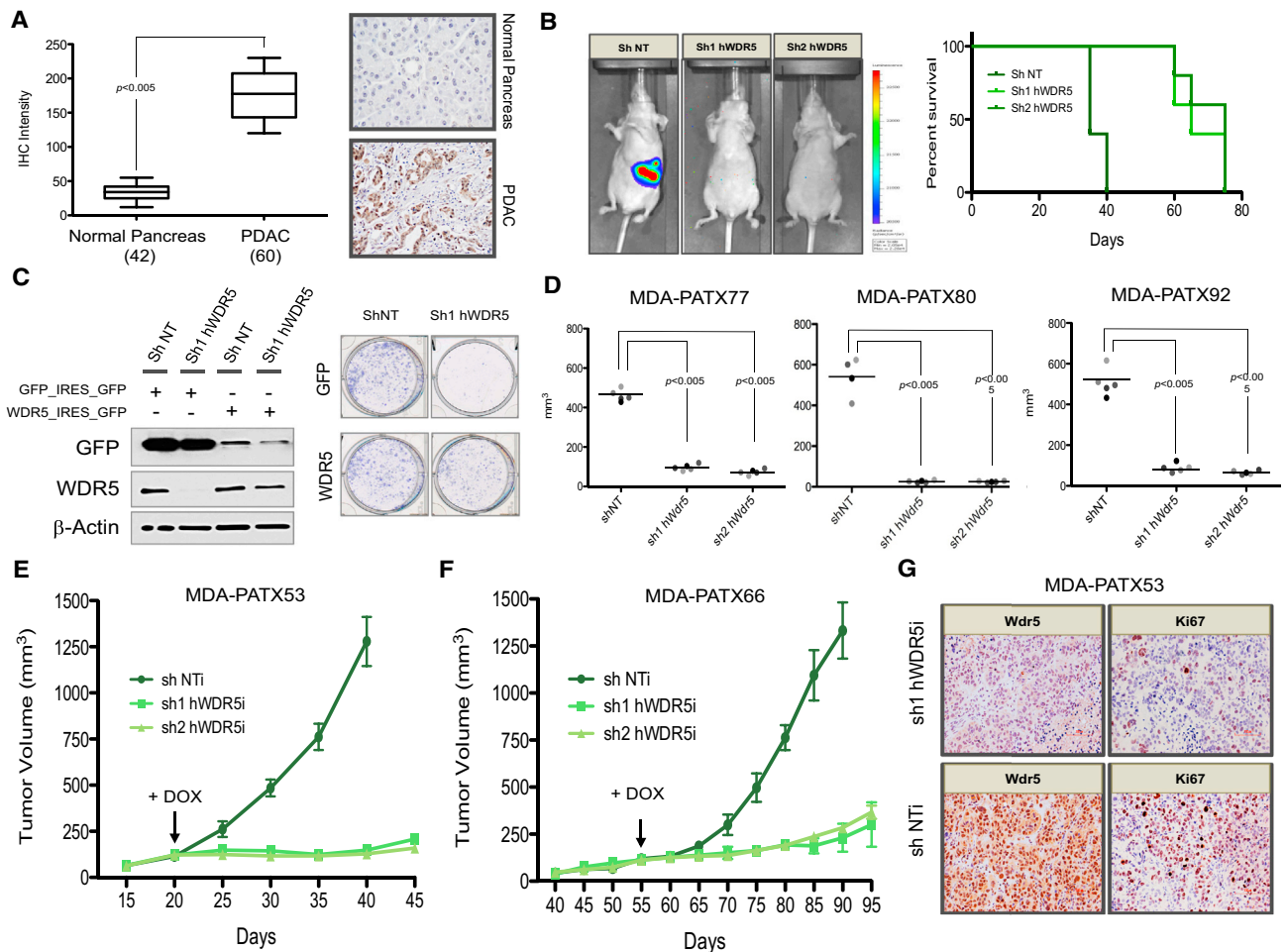
Figure 3. WDR5 Is Essential for PDAC Initiation and Proliferation

(A) Boxplot of WDR5 intensity staining (0–300, percentage of positive cells by intensity) in pancreatic ductal adenocarcinoma Tissue Micro-Array (102 cases total, 42 normal pancreas, 60 PDACs, Student's t test p < 0.005).

(B) Non-invasive bioluminescence imaging (day 30) of representative mice injected with MDA-PATX53 cells expressing shRNA targeting WDR5 (Sh1 hWDR5 and Sh2 hWDR5) and control (Sh NT); percentage survival (n = 5, Student's t test p < 0.004).

(C) Colony formation assay (CFA) of MDA-PATX53 cells expressing pHAGE-GFP_IRES_GFP or pHAGE-WDR5_IRES_GFP and shRNA targeting WDR5 (sh1_WDR5) or control (sh_NT); Protein expression of WDR5, GFP, and β-actin.

(D) Tumor measurement (mm^3) of three primary PDAC xenograft-derived cells (MDA-PATX77, MDA-PATX80, MDA-PATX92) expressing shRNAs targeting WDR5 (sh1 hWDR5, sh2 hWDR5) and control (sh NT); median (n = 5, Student's t test p < 0.005).

(E and F) Tumor-growth curve (mm^3) of xenograft-derived MDA-PATX53 and MDA-PATX66 cells carrying Tet-ON inducible WDR5 shRNAs (Sh1 hWDR5i and Sh2 hWDR5i) or control (sh NTi) (n = 5, Student's t test p < 0.03). Size measurements were performed every 5 days. Mice were subjected to doxycycline-containing drinking water regimen from day 20 (MDA-PATX53) or day 55 (MDA-PATX66) until the end of the study.

(G) Immunohistochemistry staining (Wdr5, Ki67, 10×) of tumors generated transplanting MDA-PATX53 cells carrying Tet-ON inducible WDR5 shRNA (Sh1 hWDR5i) or control (sh NTi). Mice were sacrificed 72 hr after doxycycline supplementation in the drinking water. Data are mean ± SD.

See also Figure S4.

transplanting epithelial progenitors from *Rosa26*$^{mTmG/+}$ mice, upon infection with the pLSM5-K19 lentiviral vector, we observed no tumor formation and differentiation in pancreatic acini, as demonstrated by double positivity for GFP and amylase of pancreatic sections (Figures 4B and S5B), suggesting that early embryonic liver progenitors can be reprogrammed by the host microenvironment toward a pancreatic exocrine differentiation. Instead, *R26*$^{Cag-FlpoERT2/+}$; *KRas*$^{G12D\_LSL/+}$; *Tp53*$^{L/L}$ transplants generated tumors and expressed the epithelial markers

Cytokeratin 19 and Sox9 and the pancreas-specific marker PDX1, suggesting that embryonic endodermal progenitors are remarkably adaptable and able to generate pancreatic tumors, which pathologically recapitulate the human counterpart (Figures 4C, S5C, and S5D). Upon tumor establishment, FlpoERT2 was activated by repeated tamoxifen (Tx) treatments to remove the stopper cassette and activate the shRNA (Figure 4D). Consistent with the above findings, acute inactivation of Wdr5 in vivo resulted in a dramatic increase of overall survival and
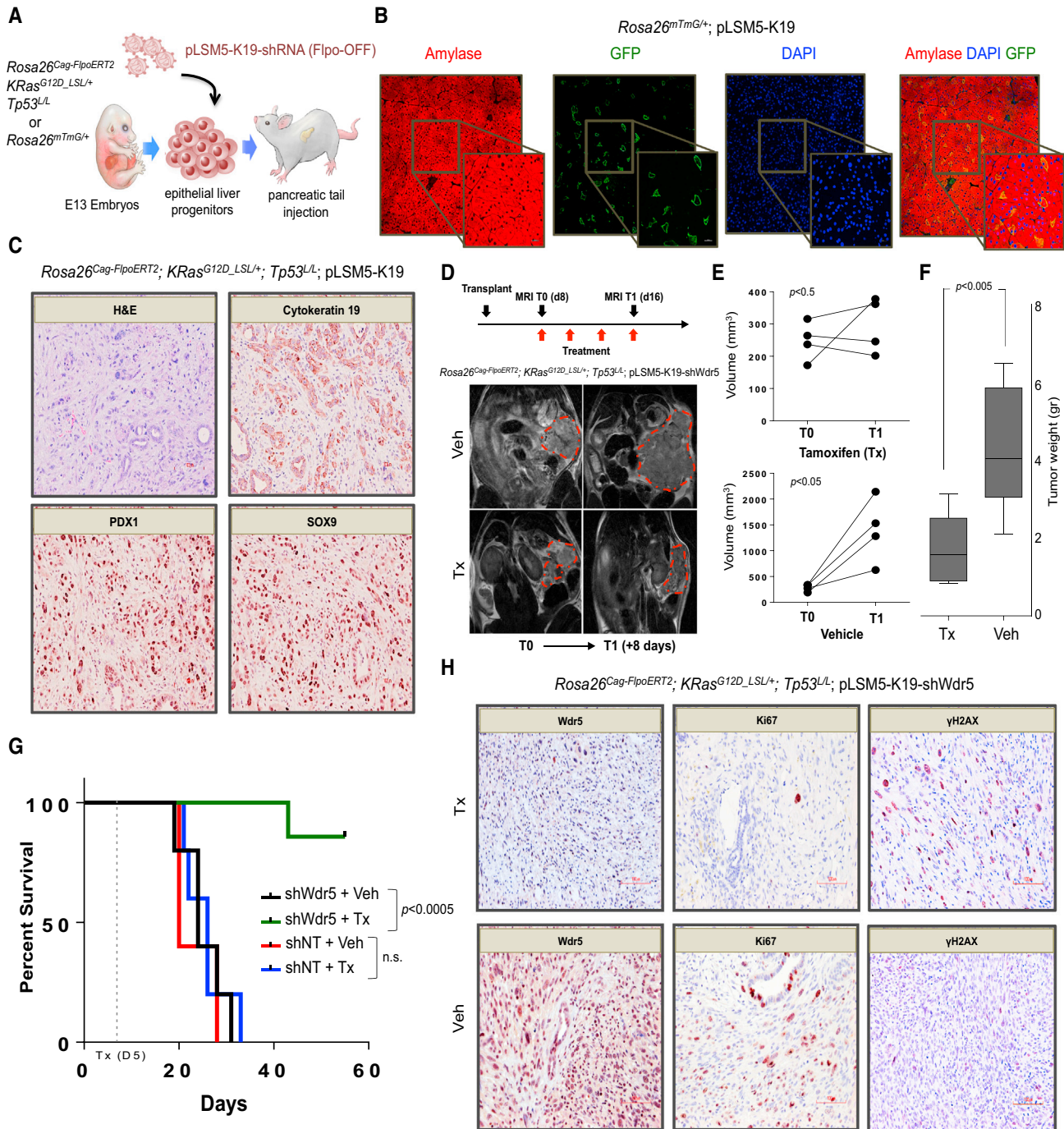
Figure 4. WDR5 Inhibition Arrests Tumor Progression of Autochthonous PDAC Models

(A) PDAC somatic mouse model experimental scheme (E13, embryonic day 13); specifically, early epithelial progenitor cultures were established from $KRas^{G12D\_LSL/+}$; $Tp53^{L/L}$; $R26^{Cag-FlpoERT2/+}$ or $Rosa26^{mTmG/+}$ embryonic livers and expanded ex vivo. Cells were transduced with the pLSM5 system and transplanted orthotopically in immunocompromised $Rag2^{-/-}$ mice.

(B) Immunofluorescence staining (Amylase, GFP, DAPI, Merge, 20×; highlighted areas, 60×) of normal pancreas collected from recipient mice transplanted with $Rosa26^{mTmG/+}$ epithelial progenitors upon infection with pLSM5-K19 (no shRNA).

(C) Immunohistochemistry staining (H&E, Cytokeratin 19, PDX1, Sox9, 20×) of tumors harvested from somatic models in the $KRas^{G12DLSL/+}$; $Tp53^{L/L}$; $R26^{Cag-FlpoERT2/+}$ background infected with pLSM5-K19 (no shRNA).

(D) Representative MRI sections of mice transplanted with $KRas^{G12DLSL/+}$; $Tp53^{L/L}$; $R26^{Cag-FlpoERT2/+}$; pLSM5-K19-shWdr5 cells randomized to vehicle (Veh) or tamoxifen (Tx) treatment. Mice were imaged at days 8 and 16 (n = 4/group). Treatment was started at day 8.

(E) Dot plots showing the individual tumor volumes at T0 and T1 time points for vehicle (ANOVA test p < 0.05) or tamoxifen (ANOVA test p < 0.5)-treated mice.

(legend continued on next page)

inhibition of tumor growth (Figures 4D–4G), characterized by a decrease in the numbers of Ki67 positive cells and accumulation of DNA damage (γH2AX staining) (Figure 4H).

The COMPASS Complex Is a Critical Regulator of PDAC Development

COMPASS and COMPASS-like complexes are characterized by their unique subunit composition, and individual subunits appear to dictate the biological functions of each complex (Trievel and Shilatifard, 2009; Smith et al., 2011). For example, even though both MLL1 and MLL2 are recruited to the Hox loci through MEN1-specific interactions, they also have non-redundant functions, as exemplified by the phenotypes of *MLL1* and *MLL2* knockout mouse models (Yu et al., 1995; Wang et al., 2009). The WDR5-RBBP5-ASH2L (WAR) core showed high protein expression level in human PDAC xenografts, associated with a hypermethylation phenotype (Figure 5A). The functional non-redundant role of the COMPASS complex in human PDAC was proved by the significant impairment of colony formation ability we observed when ASH2L, RBBP5, and MLL1 were downregulated in PDX-derived samples using two independent shRNAs (Figures 5B–5E and S6A–S6D). In addition, the downregulation of each member of the so-called WAR module (WDR5-ASH2L-RBBP5) in human PDAC models affected the expression of a set of common genes highlighting a critical role of the complex in sustaining tumor proliferation (Figure S6E; Table S3). WDR5 association with methyltransferases in the COMPASS complex leads to H3K4 methylation, a validated marker of open-chromatin conformation and active transcription (Steward et al., 2006; Trievel and Shilatifard, 2009; Smith et al., 2011; Schuettengruber et al., 2011). We thus hypothesized that knockdown of WDR5 would impact H3K4 methylation in PDAC cell lines. Using H3K4me3 chromatin immunoprecipitation sequencing (ChIP-seq), we observed a moderate overall reduction in global methylation levels in both human and mouse PDAC cells (Figures S6F and S6G). Mapping of tri-methylation profiles with functional elements of the genome confirmed that a relatively small fraction (4%–20%) of the methylation regions found altered upon WDR5 suppression was in proximity (<1 kb) of transcriptional start sites (TSSs) (Figure S6H; Table S4). These results suggest that the COMPASS complexes may orchestrate the transcriptional control of cancer-relevant genes that support PDAC maintenance. We next performed cross-species RNA sequencing (RNA-seq) analysis to inform on transcriptional changes consequent to WDR5 knockdown (Figure 5F; Table S5). To our surprise, gene set enrichment analysis (GSEA) identified genes involved in the control of DNA replication and cell-cycle progression (Figure 5G; Table S6).

WDR5 Complex Protects PDAC Cells from Replicative Stress and DNA Damage through Myc Interaction

We next performed bromodeoxyuridine (BrdU)-labeling studies in patient-derived PDAC cells and found that WDR5 knockdown resulted in a reduction in BrdU incorporation, with a paradoxical increase in overall DNA content, suggesting failure to sustain a DNA replication checkpoint (Figures 6A and S7A–S7C). It is well established that tumor cells are inherently more sensitive to S-phase perturbations, possibly due to an increased number of active replication forks and concomitant alterations in activating G1 checkpoints (Nghiem et al., 2001). Indeed, we found that treatment with the ATR inhibitor, VE-821, caused accumulation of replicative damage in the same human PDAC cell lines (Figures 6B and S7D). In both cases, the observed dramatic cell-cycle phenotype was associated with induction of DNA damage (γH2AX staining) (Figures 6C, 6D, and S7E), which we also observed upon knocking down WDR5 in vivo (Figure 4E). Subcellular protein fractionation indicated a reduction of chromatin-bound CDC45 and an increase in chromatin-bound CDT1 upon WDR5 knockdown, suggesting that prolonged stalling of replication forks may underlie the observed arrest of the replication machinery in the absence of WDR5 (Figure 6E). The analysis of the chromatin-bound fraction also highlighted a reduction in c-Myc as a consequence of WDR5 silencing. The recent exciting finding of a direct interaction between WDR5 and c-Myc could imply that WDR5 may be recruited to chromatin to execute on Myc-dependent functions in replication (Thomas et al., 2015; Sun et al., 2015). By performing immunoprecipitation experiments for exogenously expressed Flag-WDR5 or endogenous c-Myc we confirmed the physical interaction of these two proteins in PDAC cells (Figure 6F). Notably, WDR5 mutants carrying specific point mutations in the Myc binding site (L240K and V268E; Thomas et al., 2015) drew accumulation of DNA damage (γH2AX staining), similar to the effects seen upon knocking down WDR5, and most likely due to dominant-negative effects on PDAC cells (Figure 6G). The induction of DNA damage observed upon infection of PDAC cells with these WDR5 mutants also resulted in a significant impairment of new colony formation, which was not detected when overexpressing wild-type WDR5 (Figure 6H). Finally, PDAC cells showed a greater sensitivity to pharmacological inhibition of the WDR5 interaction network (OICR-9429, 5–10 μM) than the specific inhibition of the WDR5-MLL1 association (MM-401, 20–40 μM) in colony formation assays (Figure 6I).

DISCUSSION

Established cell lines and their transplanted tumors do not reflect the heterogeneity of human cancer biology and have been

(F) Weight of the tumors (grams) harvested from *Rosa26^Cag-FlpoERT2/+; KRas^G12D_LSL/+; Tp53^L/L* background mice infected with pLSM5-K19-shWdr5 and treated for 1 week with tamoxifen (Tx, n = 7) or vehicle (Veh, n = 9) (Student's t test p < 0.005).
(G) Overall survival for somatic models in the *KRas^G12D_LSL/+; Tp53^+/+; R26^Cag-FlpoERT2/+* background infected with pLSM5-K19-shWdr5, and treated for 1 week with Tamoxifen (Tx, n = 7) or vehicle (Veh, n = 5; Mantel-Cox test, p < 0.0005), or with pLSM5-K19-shNT and treated for 1 week with Tamoxifen (Tx, n = 5) or vehicle (Veh, n = 5; Mantel-Cox test, n.s., not significant).
(H) Immunohistochemistry staining (WDR5, Ki67, phospho H2AX (γH2AX), 10×) of tumors collected (at the end of the treatments) from *Rosa26^Cag-FlpoERT2/+; KRas^G12D_LSL/+; Tp53^L/L* background mice infected with pLSM5-K19-shWdr5 and treated for 1 week with Tamoxifen (Tx) or vehicle (Veh).
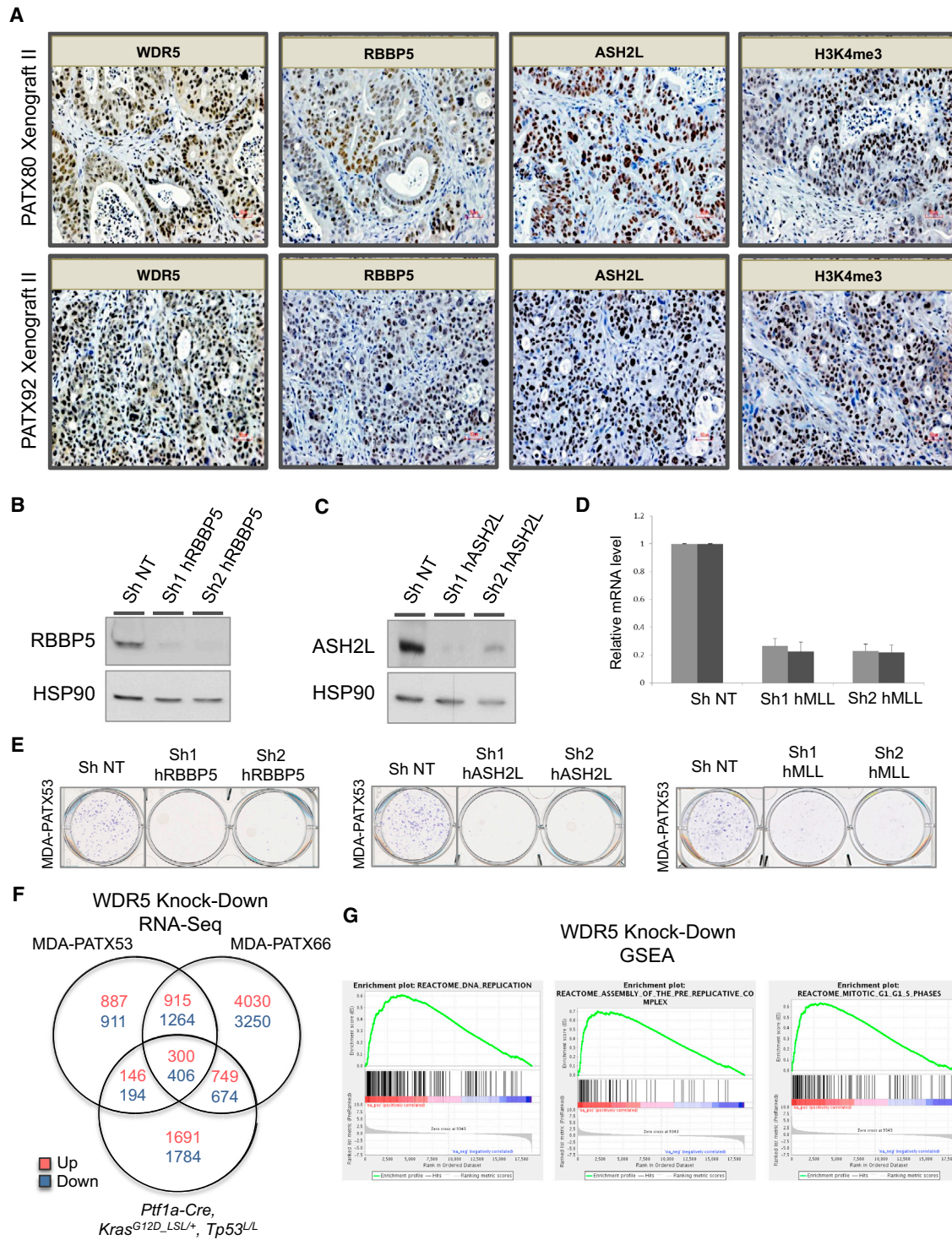See also Figure S5.

Figure 5. COMPASS Complex Subunits Are Required for PDAC Cell Proliferation

(A) Immunohistochemistry staining (WDR5, RBBP5, ASH2L, H3K4me3, 20×) of PDAC xenografts.

(B and C) Western blot of RBBP5 and ASH2L for MDA-PATX53 cells expressing shRNA targeting RBBP5 (sh1 hRBBP5, sh2 hRBBP5), ASH2L (sh1 hASH2L, sh2 hASH2L), and control (sh NT) 72 hr after infection.

(D) Bar graph shows human MLL transcript levels in MDA-PATX53 cells infected with shRNA targeting MLL (sh1 hMLL, sh2 hMLL) or control (sh NT). Transcript levels were quantified by RT-PCR 72 hr upon infection and expressed relative to mRNA levels in control (sh NT)-infected cells.

(legend continued on next page)

adapted to growth in non-physiological culture conditions. Primary cancer patient-derived xenografts are indeed able to capture a broader set of tumor cell features compared to conventional cancer cell lines, and they are being widely adopted to test efficacy of novel candidate therapeutic agents (Tentler et al., 2012). By focusing on targeting cell populations that can adequately form tumors in vivo, we move the attention to those cells required to survive upon transplantation and to sustain tumor initiation and progression (Zhou et al., 2009; Viale et al., 2014). We are aware that some of our top-scoring "hits" could have been identified using cancer cell lines, as they may be required for tumor cell proliferation, but so far no existing models could have positioned them as unbiased lethal nodes for tumor cells in a physiological context system. The stringency of our approach allows us to focus solely on most promising "hits" on which we then can perform detailed clinical-pathological and functional validation as illustrated in the case of WDR5. Our results display a critical role of WDR5 in PDAC, seemingly linked to sustaining a DNA replication checkpoint. Tumor cells possess an increased number of replication forks and endure elevated levels of replication stress compared to normal cells, opening the intriguing possibility that WDR5 overexpression in tumors may be required to stabilize the replication machinery (Figure 7) (Gaillard et al., 2015). Our observations are particularly intriguing considering the prominent role of ATR in S-phase checkpoint activation and premature chromosome condensation (PCC) in the presence of replication-associated DNA damage and absence of controlling G1 checkpoints (Nghiem et al., 2001). Here, the confirmation of a direct and functional interaction between WDR5 and c-Myc clearly demonstrated that WDR5 is critical to recruit c-Myc on the chromatin and to enable Myc-dependent tumorigenic mechanisms in PDAC (Dominguez-Sola et al., 2007; Thomas et al., 2015). The role played by Myc in transformation and cell-cycle regulation has been known for many years, as well as its stabilization by oncogenic pathways (Dang, 1999; Sears et al., 1999). In PDAC, where mutations of Kras happen at a significantly high frequency, Myc is required downstream of the MAPK cascade to sustain tumorigenesis (Ischenko et al., 2014; Stellas et al., 2014), and its knockdown in Kras-driven pancreatic cells also reduced the expression of metabolic genes critical for tumor maintenance (Ying et al., 2012). The ability of Myc to promote cellular proliferation in S-phase appears to occur through cooperation of effects, some direct, e.g., those driving the regulation of nucleotide biosynthetic pathways and the control of active replication forks, others dependent on transcriptional activation, e.g., regulation of cell-cycle genes (Campaner and Amati, 2012). In our experiments, one of the Myc controlled mechanisms that emerge to restrain replication stress is the ATR/Chk1 pathway (Murga et al., 2011; Schoppy et al., 2012), which appears to support rather than suppress tumor development. Whether this is a direct effect of WDR5 (or a WDR5-Myc complex) binding or an indirect effect possibly mediated through Myc regulated genes by a COMPASS or COMPASS-like complex, as demonstrated in neuroblastoma (Sun et al., 2015), cannot be determined from our current studies. The findings of MLL being phosphorylated and activated by ATR in order to allow for full activation of the S-phase checkpoint further highlight the functional interplay between oncogene-induced DDR and COMPASS complex (Liu et al., 2010). Our preliminary experiments with two available low potency WDR5 inhibitors supported the centrality of the WDR5 network (OICR-9429), more than MLL-specific associations (MM-401), in driving PDAC cell proliferation, but also highlighted the requirement for a new generation of potent and selective Myc-oriented WDR5 inhibitors to deeply dissect the WDR5-Myc molecular dynamics and accelerate the bench-to-bedside translation process (Grebien et al., 2015; Cao et al., 2014). In further support of our mechanistic findings, it was previously demonstrated that ATR inhibition sensitizes PDAC cell lines to radiation or chemotherapy (Prevo et al., 2012).

Here, we also describe a highly efficient technology for the rapid in vivo validation of any gene function in GEMM-derived models of PDAC. Compared to the traditional validation methods (constitutive or inducible RNAi tools), it has the advantage of knocking down a gene of interest in a time-restricted manner, in autochthonous pancreatic tumors originated from reprogrammed embryonic progenitors. It should be kept in mind that this system has some intrinsic limitations, as the oncogene activation ($Kras^{G12D}$) and the inactivation of $Tp53$ are achieved in E12.5/E13 liver progenitors, which, in spite of their remarkable plasticity and their ability to express markers of pancreatic terminal differentiation upon transplantation, may still retain some features of the embryonic tissue of origin and potentially generate cholangiocarcinoma-like lesions.

Taken together, our data highlight this approach as a powerful platform for the rapid identification of genetic vulnerabilities using patient-derived tumor samples. While here we chose to characterize common hits across multiple tumors, the systematic evaluation of epigenetic regulators in specific genetic contexts and tumor molecular subtypes is certainly possible. This platform can also be enabled in syngeneic mouse models or humanized mice where one can probe the effects of target inhibition in the context of an intact immune response and in the presence of immune checkpoint activators.

EXPERIMENTAL PROCEDURES

Tumor Cell Isolation and Culture from Human PDx

Tumors from human primary xenografts (Xenograft I) were harvested in HBSS (Gibco). Isolation of pancreatic adenocarcinoma tumor xenograft (PATX) cells was performed by a combination of enzymatic (Tumor Dissociation Kit, human, Miltenyi Biotec) and mechanical (mincing the tumor tissue in very small pieces with sterile scissors) dissociation protocols. The single-cell populations

---

(E) Colony formation assay (CFA) for MDA-PATX53 cells expressing shRNA targeting RBBP5 (sh1 hRBBP5, sh2 hRBBP5, left panel), ASH2L (sh1 hASH2L, sh2 hASH2L, middle panel), MLL (sh1 hMLL, sh2 hMLL, right panel), and control (sh NT).
(F) Venn diagram of the genes differentially expressed in human and mouse PDAC models upon WDR5 knockdown (RNA-seq replicates, FC >1.5, FDR 1%).
(G) Gene set enrichment analysis (GSEA) of differentially expressed (DE) genes upon WDR5 knockdown; Merge of the human and mouse PDAC cells infected with two independent shRNA targeting WDR5 or control (sh NT) 72 hr after infection. Data are mean ± SD.
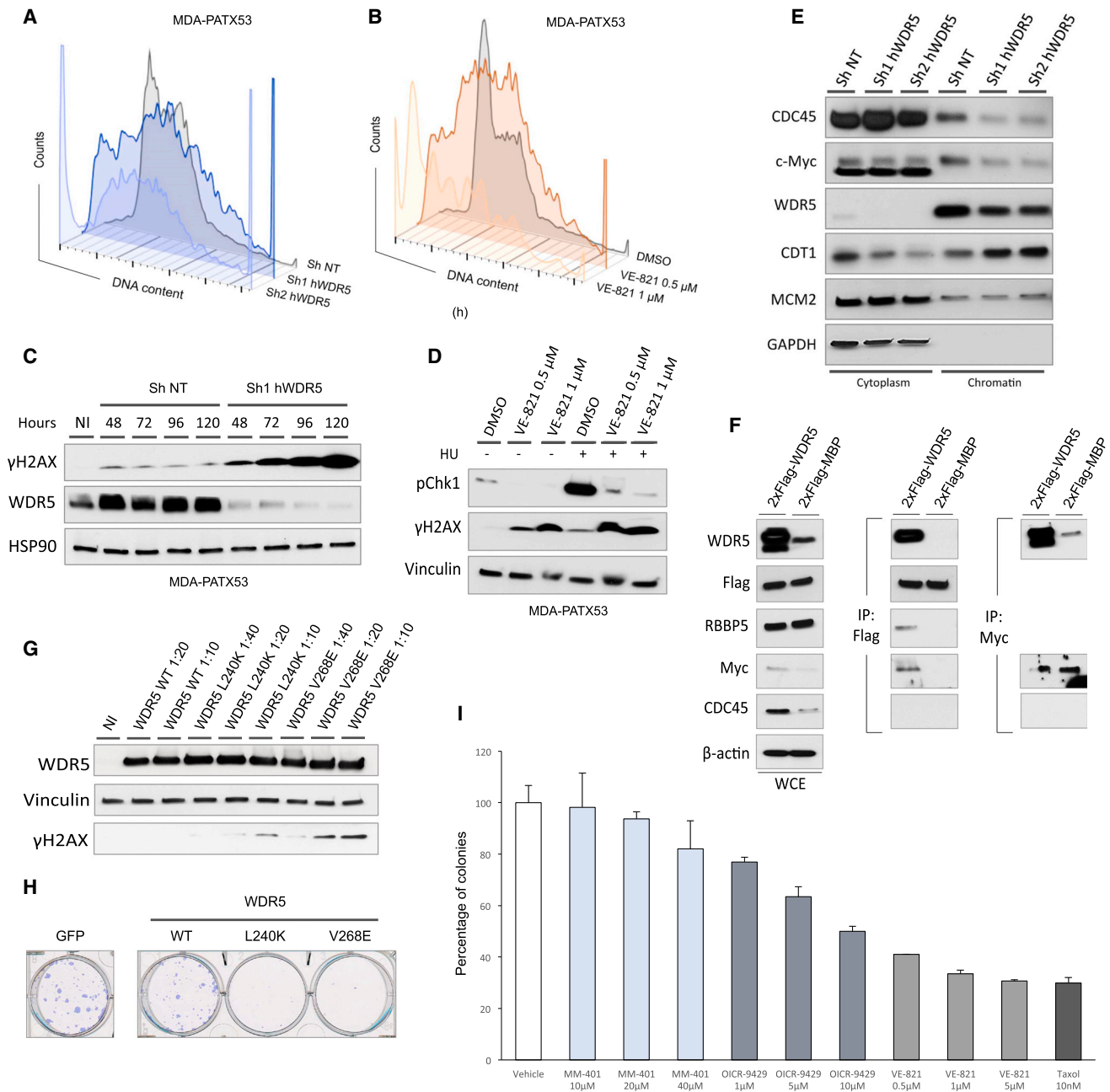See also Figure S6 and Tables S3–S6.

Figure 6. WDR5 Complex Protects PDAC Cells from Replicative Stress and DNA Damage through c-Myc

(A and B) DNA content analysis (DAPI) by flow cytometry for MDA-PATX53 cells infected with two independent shRNA targeting WDR5 (120 hr after infection) or treated with ATR inhibitor VE-821 (0.5 and 1 μM, vehicle 0.1% DMSO) and collected 72 hr after drug addiction.

(C) Western blot for MDA-PATX53 cells expressing shRNA targeting WDR5 (sh1 hWDR5) and control (sh NT) at different time points after infection (48, 72, 96, 120 hr; NI, not infected); protein expression of phospho-H2AX (γH2AX), WDR5, and HSP90.

(D) Western blot for MDA-PATX53 cells treated for 72 hr with two different concentrations (0.5 and 1 μM) of the ATR inhibitor (VE-821) or vehicle (0.1% DMSO); cells were harvested upon 1 hr treatment with (+) or without (–) Hydroxyurea (HU); protein expression of phospho-Chk1 (Ser345), phospho H2AX (γH2AX), and Vinculin.

(E) Subcellular protein fractionation (cytoplasmic and chromatin-bound fractions) of MDA-PATX53 cells infected with two independent shRNA for WDR5 (Sh1 hWDR5, Sh2 hWDR5) or control (Sh NT) and collected 48 hr upon infection. Protein expression of CDC45, WDR5, CDT1, Myc, MCM2, and GAPDH.

(F) Immunoprecipitation (IP) of WDR5-Myc in MDA-PATX53 PDAC cells: whole-cell extracts (WCE, 0.5% input) collected from cells infected with pHAGE-2xFlag-WDR5 or pHAGE-2xFlag-MBP (maltose-binding protein) (left panel); IP of the 2xFlag tag for the cells infected with pHAGE-2xFlag-WDR5 or pHAGE-2xFlag-MBP (central panel, 1/15 of the eluates); IP of endogenous Myc for the cells infected with pHAGE-2xFlag-WDR5 or pHAGE-2xFlag-MBP (right panel, 1/15 of the eluates), protein expression of WDR5, Flag, RBBP5, Myc, CDC45, and β-actin.

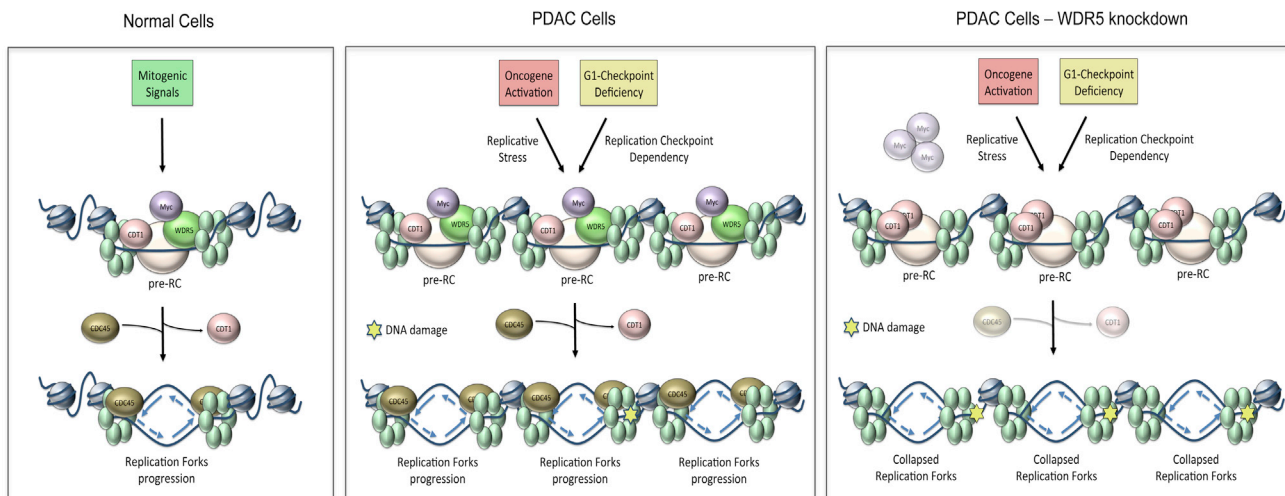*(legend continued on next page)*

Normal Cells   PDAC Cells   PDAC Cells – WDR5 knockdown

Figure 7. WDR5 Is Critical to Sustain c-Myc Proliferative Functions in PDAC Cells

WDR5-Myc interaction regulates cell proliferation and DNA replication forks progression in normal non-tumorigenic cells or PDAC cells, through transcriptional and non-transcriptional mechanisms. In PDAC, the presence of an activated oncogene (frequently Kras), driving c-Myc stabilization, and the absence of proficient G1 checkpoint (p53 or p16 alterations) impose increased number of replication forks and elevated levels of replication stress compared to normal cells. In this situation, disruption of the WDR5-Myc association sensitizes the pancreatic cancer cell to DNA damage accumulation and replication forks collapse.

were seeded at high confluency on collagen-IV-coated plates (Corning) in DMEM/F12 (Gibco) supplemented with 10% fetal bovine serum (FBS) (Gibco), 1% BSA (Fisher Scientific), 0.5 μM hydrocortisone (Sigma-Aldrich), 10 mM HEPES (Invitrogen), 100 ng/ml cholera toxin (Sigma-Aldrich), 5 ml/l insulin-transferrin-selenium (BD), 100 IU/ml penicillin (Gibco), and 100 μg/ml streptomycin (Gibco). In order to get rid of the murine fibroblasts in the culture, we performed brief trypsinization cycles (0.25% Trypsin-EDTA, Gibco). The enrichment for human components was confirmed by flow cytometry comparing the percentage of cells expressing human (HLA-ABC) or mouse (H-2Kd) histocompatibility complex antigens. The isolated human cells were maintained in culture for a maximum of three passages before being transplanted in a secondary host (Xenograft II).

Libraries Design and Construction

A custom library constituted by 2,410 shRNAs focused on chromatin remodeling enzymes was constructed by using chip-based oligonucleotide synthesis and cloned into the pRSI16 lentiviral vector (Cellecta) as a pool. The shRNA library targeted 236 genes with coverage of 10 shRNAs/gene. The shRNA includes two G/U mismatches in the passenger strand, a 7-nt loop and a 21-nt targeting sequence. Targeting sequences were designed using a proprietary algorithm (Cellecta). The oligo corresponding to each shRNA was synthesized with a unique molecular barcode (18 nucleotides) for measuring representation by NGS. The 12.5k barcoded library applied for the engraftment efficiency studies was constructed using the same technology and cloned as a pool into the pRSI17 lentiviral plasmid (Cellecta).

In Vivo Engraftment Efficiency Studies

The volume of virus required to give a percentage of infection around 30% or below was determined sample by samples using a three-point dose response

in the presence of 8 μg/ml polybrene (Millipore): 0.15, 0.3, and 0.6 transducing unit (TU)/cell for the human PDx cells; 0.3, 0.6, and 1.2 TU/cell for the GEMM-derived cells (see Figure S2). Infectivity was determined as the percentage of RFP positive cells 2 days after infection as measured by fluorescence-activated cell sorting (FACS) analysis. For large-scale infection of human PDx and mouse GEMM-derived cells, 60 or 20 million cells were, respectively, plated in T-175 flasks (Corning) with fresh media containing 8 μg/ml polybrene and sufficient virus to guarantee a 15%–25% infection rate based on precedent calculations. For each cell line, the optimal puromycin dose to achieve more than 95% cell killing in 72 hr was determined by measuring cell viability with a Cell Titer Glo assay (Promega) for a six-point dose response ranging from 0 to 8 μg of puromycin. 72 hr following puromycin addiction, cells were trypsinized, pooled together, and counted. A representative portion of the total cells (normally one-third or one-fourth) was collected as reference cells and immediately frozen as pellet at −80°C. The cells for the in vivo studies were separated into independent tubes (replicates or triplicates), suspended in 200 μl of a PBS:Matrigel (1:1) solution and injected subcutaneously into the flank of 4- to 6-week-old female immunocompromised mice (NSG, The Jackson Laboratory). The experiments with the GEMM-derived cells were performed transplanting 10^6 cells per mouse ensuring an in vivo representation of 80 cells/barcode. For the human PDx experiments, each injection was performed with 5×10^6 cells to guarantee an in vivo coverage of 400 cells/barcode. Specifically, the engraftment efficiency study with the MDA-PATX53 to modulate the appropriate coverage was executed in triplicate with 10^6, 3×10^6 and 5×10^6 cells from the same infection. Mice were monitored every 5 days and euthanized when the tumors reached a volume around 750 mm^3 as determined by caliper measurement. Tumor volume was calculated using the formula: V = l^2*L/2 (l, length; L, width). The whole tumor was collected from each mouse under sterile conditions, weighed, and snap-frozen in liquid nitrogen.

(G and H) Western blot for MDA-PATX53 cells infected with different dilutions (1:40, 1:20, and 1:10) of pHAGE-WDR5 wild-type (WT) or mutants in the Myc-binding site (L240K, V268E) and collected 48 hr after infection (NI, not infected), Protein expression of phospho-H2AX (γH2AX), WDR5 and Vinculin (upper panel); colony formation assay (CFA) of MDA-PATX53 cells expressing pHAGE-GFP, pHAGE-WDR5 wild-type (WT) or pHAGE-WDR5 mutants (L240K, V268E) upon infection with 1:20 of the lentiviral preparation (lower panel).

(I) Colony formation assay (CFA) of MDA-PATX53 cells in response to OICR-9429, MM-401, and VE-821 at indicated concentrations (Taxol has been used in these experiments as positive control, 10 nM). Numbers were normalized to colonies generated in response to 0.1% DMSO (vehicle). Data are mean ± SD. See also Figure S7.

In Vivo shRNA Screens

Infectivity was determined sample by sample as the percentage of GFP positive cells 2 days after infection as measured by FACS analysis. For large-scale infection of human PDx and mouse GEMM-derived cells the same experimental procedure described above has been applied (see In Vivo Engraftment Efficiency Studies). The experiments with the GEMM-derived cells were performed transplanting 10^6 cells per mouse ensuring an in vivo representation of 400 cells/barcode. For the human PDx experiments, each injection was performed with 5×10^6 cells to guarantee an in vivo coverage of 2,000 cells/barcode.

Bioinformatics and Data Analysis

Read Counting

Illumina base calls were processed using CASAVA (v.1.8.2), and resulting reads were processed using our in-house pipeline. Raw FASTQ files are filtered for a 4-bp spacer (CGAA) starting at 18th base allowing for one mismatch, such that only reads amplified using above mentioned PCRs are used for further processing. We then extract 23–40 bp of the above reads for targeting libraries, and 1–18 bp for non-targeting library. These are further aligned using Bowtie (2.0.2) to their respective libraries (2.4k mouse Epigenome, 2.4k human Epigenome, and 12.5k non-targeting library) (Langmead et al., 2009). We then use SAMtools to count the number of reads aligned to each barcode (Li et al., 2009).

Engraftment Efficiency Analysis

Read counts are normalized for the amount of sequencing reads retrieved for each sample, using library size normalization (to 100 million reads).

Screen Hit Analysis

A similar approach was employed as with engraftment efficiency analysis, described above. Using normalized counts, each sample is compared with its respective reference and a Log_2 fold change (FC) is calculated. This is further normalized using a robust Z score defined by (FC – Median)/Median absolute deviation (MAD) (König et al., 2007). To summarize the effect of knockdown at gene level we employed RSA, to score each gene (Birmingham et al., 2009).

Somatic Lentiviral Vectors and Other Plasmids

pLSM5: a synthetic cassette (Geneart, Life Technologies) containing the U6 promoter and the Cre recombinase sequence under the human Keratin 19 promoter (−1114, +141) flanked by two TATA-Frt sites (XbaI-U6-TATA-Frt-EcoRI-hKrt19-NheI-Cre-TATA-Frt-HpaI) was cloned into the XbaI/HpaI site of the pSICO vector. A DNA fragment was liberated by XbaI/KpnI digestion and cloned into the XbaI/KpnI sites of the pLB vector 32. The introduction of the TATA box into the Frt sites was designed according to Ventura et al. (2004). All the constructs were verified by restriction digestion and sequencing. The pSICO and pSICO-Flpo were made by Dr. Tyler Jacks (Ventura et al., 2007). The pLB vector was created by Dr. Stephan Kissler. All plasmids were obtained through Addgene.

Lentiviral Somatic Mosaic GEM Model

Embryonic liver progenitors (E12.5/E13) were isolated and cultured according to Zender et al. (2008). Cells were infected 24 hr after seeding with the pLSM5 virus, and 2×10^5 cells were injected in the tail of the pancreas of $Rag2^{-/-}$ mice. Before cell injection, $Rag2^{-/-}$ mice, approximately 8–10 weeks old, received seven consecutive (one each day) intraperitoneal injections of cerulein (10 μg/kg) according to Morris et al. (2010). Animals were monitored weekly for tumor formation. Tumor-bearing mice were injected intraperitoneally every other day with Tamoxifen (5×100-μl injections, 15 mg/ml).

ACCESSION NUMBERS

The accession number for the RNA-seq and ChIP-seq data reported in this paper is European Genome-Phenome Archive (EGA): PRJEB13892.

SUPPLEMENTAL INFORMATION

Supplemental Information includes Supplemental Experimental Procedures, seven figures, and six tables and can be found with this article online at http://dx.doi.org/10.1016/j.celrep.2016.05.063.

REFERENCES

Almoguera, C., Shibata, D., Forrester, K., Martin, J., Arnheim, N., and Perucho, M. (1988). Most human carcinomas of the exocrine pancreas contain mutant c-K-ras genes. Cell 53, 549–554.

American Cancer Society. (2015). Cancer Facts & Figures.

Baratta, M.G., Schinzel, A.C., Zwang, Y., Bandopadhayay, P., Bowman-Colin, C., Kutt, J., Curtis, J., Piao, H., Wong, L.C., Kung, A.L., et al. (2015). An in-tumor genetic screen reveals that the BET bromodomain protein, BRD4, is a potential therapeutic target in ovarian carcinoma. Proc. Natl. Acad. Sci. USA 112, 232–237.

Biankin, A.V., Waddell, N., Kassahn, K.S., Gingras, M.C., Muthuswamy, L.B., Johns, A.L., Miller, D.K., Wilson, P.J., Patch, A.M., Wu, J., et al.; Australian Pancreatic Cancer Genome Initiative (2012). Pancreatic cancer genomes reveal aberrations in axon guidance pathway genes. Nature 491, 399–405.

Birmingham, A., Selfors, L.M., Forster, T., Wrobel, D., Kennedy, C.J., Shanks, E., Santoyo-Lopez, J., Dunican, D.J., Long, A., Kelleher, D., et al. (2009). Statistical methods for analysis of high-throughput RNA interference screens. Nat. Methods 6, 569–575.

Bonnefoix, T., and Callanan, M. (2010). Revisiting the concept of phenotypically distinct malignant pancreatic stem-cell subsets based on limiting dilution transplantation assays. J. Clin. Oncol. 28, e89–e90.

Campaner, S., and Amati, B. (2012). Two sides of the Myc-induced DNA damage response: from tumor suppression to tumor maintenance. Cell Div. 7, 6.

Cao, F., Townsend, E.C., Karatas, H., Xu, J., Li, L., Lee, S., Liu, L., Chen, Y., Ouillette, P., Zhu, J., et al. (2014). Targeting MLL1 H3K4 methyltransferase activity in mixed-lineage leukemia. Mol. Cell 53, 247–261.

Chen, X., Xie, W., Gu, P., Cai, Q., Wang, B., Xie, Y., Dong, W., He, W., Zhong, G., Lin, T., and Huang, J. (2015). Upregulated WDR5 promotes proliferation, self-renewal and chemoresistance in bladder cancer via mediating H3K4 trimethylation. Sci. Rep. 5, 8293.

Conroy, T., Desseigne, F., Ychou, M., Bouché, O., Guimbaud, R., Bécouarn, Y., Adenis, A., Raoul, J.L., Gourgou-Bourgade, S., de la Fouchardière, C., et al.; Groupe Tumeurs Digestives of Unicancer; PRODIGE Intergroup

(2011). FOLFIRINOX versus gemcitabine for metastatic pancreatic cancer. N. Engl. J. Med. *364*, 1817–1825.

Dang, C.V. (1999). c-Myc target genes involved in cell growth, apoptosis, and metabolism. Mol. Cell. Biol. *19*, 1–11.

Dawson, M.A., and Kouzarides, T. (2012). Cancer epigenetics: from mechanism to therapy. Cell *150*, 12–27.

Dominguez-Sola, D., Ying, C.Y., Grandori, C., Ruggiero, L., Chen, B., Li, M., Galloway, D.A., Gu, W., Gautier, J., and Dalla-Favera, R. (2007). Non-transcriptional control of DNA replication by c-Myc. Nature *448*, 445–451.

Gaillard, H., García-Muse, T., and Aguilera, A. (2015). Replication stress and cancer. Nat. Rev. Cancer *15*, 276–289.

Grebien, F., Vedadi, M., Getlik, M., Giambruno, R., Grover, A., Avellino, R., Skucha, A., Vittori, S., Kuznetsova, E., Smil, D., et al. (2015). Pharmacological targeting of the Wdr5-MLL interaction in C/EBPα N-terminal leukemia. Nat. Chem. Biol. *11*, 571–578.

Hingorani, S.R., Petricoin, E.F., Maitra, A., Rajapakse, V., King, C., Jacobetz, M.A., Ross, S., Conrads, T.P., Veenstra, T.D., Hitt, B.A., et al. (2003). Preinvasive and invasive ductal pancreatic cancer and its early detection in the mouse. Cancer Cell *4*, 437–450.

Hingorani, S.R., Wang, L., Multani, A.S., Combs, C., Deramaudt, T.B., Hruban, R.H., Rustgi, A.K., Chang, S., and Tuveson, D.A. (2005). $Trp53^{R172H}$ and $Kras^{G12D}$ cooperate to promote chromosomal instability and widely metastatic pancreatic ductal adenocarcinoma in mice. Cancer Cell *7*, 469–483.

Hoffman, G.R., Rahal, R., Buxton, F., Xiang, K., McAllister, G., Frias, E., Bagdasarian, L., Huber, J., Lindeman, A., Chen, D., et al. (2014). Functional epigenetics approach identifies BRM/SMARCA2 as a critical synthetic lethal target in BRG1-deficient cancers. Proc. Natl. Acad. Sci. USA *111*, 3128–3133.

Hu, Y., and Smyth, G.K. (2009). ELDA: extreme limiting dilution analysis for comparing depleted and enriched populations in stem cell and other assays. J. Immunol. Methods *347*, 70–78.

Hubert, C.G., Bradley, R.K., Ding, Y., Toledo, C.M., Herman, J., Skutt-Kakaria, K., Girard, E.J., Davison, J., Berndt, J., Corrin, P., et al. (2013). Genome-wide RNAi screens in human brain tumor isolates reveal a novel viability requirement for PHF5A. Genes Dev. *27*, 1032–1045.

Ischenko, I., Petrenko, O., and Hayman, M.J. (2014). Analysis of the tumor-initiating and metastatic capacity of PDX1-positive cells from the adult pancreas. Proc. Natl. Acad. Sci. USA *111*, 3466–3471.

Ishizawa, K., Rasheed, Z.A., Karisch, R., Wang, Q., Kowalski, J., Susky, E., Pereira, K., Karamboulas, C., Moghal, N., Rajeshkumar, N.V., et al. (2010). Tumor-initiating cells are rare in many human tumors. Cell Stem Cell *7*, 279–282.

Kim, J.Y., Banerjee, T., Vinckevicius, A., Luo, Q., Parker, J.B., Baker, M.R., Radhakrishnan, I., Wei, J.J., Barish, G.D., and Chakravarti, D. (2014). A role for WDR5 in integrating threonine 11 phosphorylation to lysine 4 methylation on histone H3 during androgen signaling and in prostate cancer. Mol. Cell *54*, 613–625.

König, R., Chiang, C.Y., Tu, B.P., Yan, S.F., DeJesus, P.D., Romero, A., Bergauer, T., Orth, A., Krueger, U., Zhou, Y., and Chanda, S.K. (2007). A probability-based approach for the analysis of large-scale RNAi screens. Nat. Methods *4*, 847–849.

Krattenmacher, A., et al. (2014). Synthetic lethality screen identifies SMC2 as a new target gene in pancreatic cancer. Pancreatology *13*, S66.

Langmead, B., Trapnell, C., Pop, M., and Salzberg, S.L. (2009). Ultrafast and memory-efficient alignment of short DNA sequences to the human genome. Genome Biol. *10*, R25.

Li, H., Handsaker, B., Wysoker, A., Fennell, T., Ruan, J., Homer, N., Marth, G., Abecasis, G., and Durbin, R.; 1000 Genome Project Data Processing Subgroup (2009). The Sequence alignment/map (SAM) format and SAMtools. Bioinformatics *25*, 2078–2079.

Liu, H., Takeda, S., Kumar, R., Westergard, T.D., Brown, E.J., Pandita, T.K., Cheng, E.H., and Hsieh, J.J. (2010). Phosphorylation of MLL by ATR is required for execution of mammalian S-phase checkpoint. Nature *467*, 343–346.

Meacham, C.E., Ho, E.E., Dubrovsky, E., Gertler, F.B., and Hemann, M.T. (2009). *In vivo* RNAi screening identifies regulators of actin dynamics as key determinants of lymphoma progression. Nat. Genet. *41*, 1133–1137.

Moffat, J., Grueneberg, D.A., Yang, X., Kim, S.Y., Kloepfer, A.M., Hinkle, G., Piqani, B., Eisenhaure, T.M., Luo, B., Grenier, J.K., et al. (2006). A lentiviral RNAi library for human and mouse genes applied to an arrayed viral high-content screen. Cell *124*, 1283–1298.

Morris, J.P., 4th, Cano, D.A., Sekine, S., Wang, S.C., and Hebrok, M. (2010). Beta-catenin blocks Kras-dependent reprogramming of acini into pancreatic cancer precursor lesions in mice. J. Clin. Invest. *120*, 508–520.

Murga, M., Campaner, S., Lopez-Contreras, A.J., Toledo, L.I., Soria, R., Montaña, M.F., D'Artista, L., Schleker, T., Guerra, C., Garcia, E., et al. (2011). Exploiting oncogene-induced replicative stress for the selective killing of Myc-driven tumors. Nat. Struct. Mol. Biol. *18*, 1331–1335.

Nghiem, P., Park, P.K., Kim, Y., Vaziri, C., and Schreiber, S.L. (2001). ATR inhibition selectively sensitizes G1 checkpoint-deficient cells to lethal premature chromatin condensation. Proc. Natl. Acad. Sci. USA *98*, 9092–9097.

Omura, N., and Goggins, M. (2009). Epigenetics and epigenetic alterations in pancreatic cancer. Int. J. Clin. Exp. Pathol. *2*, 310–326.

Possemato, R., Marks, K.M., Shaul, Y.D., Pacold, M.E., Kim, D., Birsoy, K., Sethumadhavan, S., Woo, H.K., Jang, H.G., Jha, A.K., et al. (2011). Functional genomics reveal that the serine synthesis pathway is essential in breast cancer. Nature *476*, 346–350.

Possik, P.A., Müller, J., Gerlach, C., Kenski, J.C., Huang, X., Shahrabi, A., Krijgsman, O., Song, J.Y., Smit, M.A., Gerritsen, B., et al. (2014). Parallel *in vivo* and *in vitro* melanoma RNAi dropout screens reveal synthetic lethality between hypoxia and DNA damage response inhibition. Cell Rep. *9*, 1375–1386.

Prevo, R., Fokas, E., Reaper, P.M., Charlton, P.A., Pollard, J.R., McKenna, W.G., Muschel, R.J., and Brunner, T.B. (2012). The novel ATR inhibitor VE-821 increases sensitivity of pancreatic cancer cells to radiation and chemotherapy. Cancer Biol. Ther. *13*, 1072–1081.

Quintana, E., Shackleton, M., Sabel, M.S., Fullen, D.R., Johnson, T.M., and Morrison, S.J. (2008). Efficient tumour formation by single human melanoma cells. Nature *456*, 593–598.

Sahai, V., Kumar, K., Knab, L.M., Chow, C.R., Raza, S.S., Bentrem, D.J., Ebine, K., and Munshi, H.G. (2014). BET bromodomain inhibitors block growth of pancreatic cancer cells in three-dimensional collagen. Mol. Cancer Ther. *13*, 1907–1917.

Schlabach, M.R., Luo, J., Solimini, N.L., Hu, G., Xu, Q., Li, M.Z., Zhao, Z., Smogorzewska, A., Sowa, M.E., Ang, X.L., et al. (2008). Cancer proliferation gene discovery through functional genomics. Science *319*, 620–624.

Scholl, C., Fröhling, S., Dunn, I.F., Schinzel, A.C., Barbie, D.A., Kim, S.Y., Silver, S.J., Tamayo, P., Wadlow, R.C., Ramaswamy, S., et al. (2009). Synthetic lethal interaction between oncogenic KRAS dependency and STK33 suppression in human cancer cells. Cell *137*, 821–834.

Schoppy, D.W., Ragland, R.L., Gilad, O., Shastri, N., Peters, A.A., Murga, M., Fernandez-Capetillo, O., Diehl, J.A., and Brown, E.J. (2012). Oncogenic stress sensitizes murine cancers to hypomorphic suppression of ATR. J. Clin. Invest. *122*, 241–252.

Schuettengruber, B., Martinez, A.M., Iovino, N., and Cavalli, G. (2011). Trithorax group proteins: switching genes on and keeping them active. Nat. Rev. Mol. Cell Biol. *12*, 799–814.

Sears, R., Leone, G., DeGregori, J., and Nevins, J.R. (1999). Ras enhances Myc protein stability. Mol. Cell *3*, 169–179.

Silva, J.M., Marran, K., Parker, J.S., Silva, J., Golding, M., Schlabach, M.R., Elledge, S.J., Hannon, G.J., and Chang, K. (2008). Profiling essential genes in human mammary cells by multiplex RNAi screening. Science *319*, 617–620.

Smith, E., Lin, C., and Shilatifard, A. (2011). The super elongation complex (SEC) and MLL in development and disease. Genes Dev. *25*, 661–672.

Stathis, A., and Moore, M.J. (2010). Advanced pancreatic carcinoma: current treatment and future challenges. Nat. Rev. Clin. Oncol. *7*, 163–172.

Stellas, D., Szabolcs, M., Koul, S., Li, Z., Polyzos, A., Anagnostopoulos, C., Cournia, Z., Tamvakopoulos, C., Klinakis, A., and Efstratiadis, A. (2014).

Therapeutic effects of an anti-Myc drug on mouse pancreatic cancer. J. Natl. Cancer Inst. 106, dju320.

Steward, M.M., Lee, J.S., O'Donovan, A., Wyatt, M., Bernstein, B.E., and Shilatifard, A. (2006). Molecular regulation of H3K4 trimethylation by ASH2L, a shared subunit of MLL complexes. Nat. Struct. Mol. Biol. 13, 852–854.

Sun, Y., Bell, J.L., Carter, D., Gherardi, S., Poulos, R.C., Milazzo, G., Wong, J.W., Al-Awar, R., Tee, A.E., Liu, P.Y., et al. (2015). WDR5 supports an N-Myc transcriptional complex that drives a protumorigenic gene expression signature in neuroblastoma. Cancer Res. 75, 5143–5154.

Tentler, J.J., Tan, A.C., Weekes, C.D., Jimeno, A., Leong, S., Pitts, T.M., Arcaroli, J.J., Messersmith, W.A., and Eckhardt, S.G. (2012). Patient-derived tumour xenografts as models for oncology drug development. Nat. Rev. Clin. Oncol. 9, 338–350.

Thomas, L.R., Wang, Q., Grieb, B.C., Phan, J., Foshage, A.M., Sun, Q., Olejniczak, E.T., Clark, T., Dey, S., Lorey, S., et al. (2015). Interaction with WDR5 promotes target gene recognition and tumorigenesis by MYC. Mol. Cell 58, 440–452.

Trievel, R.C., and Shilatifard, A. (2009). WDR5, a complexed protein. Nat. Struct. Mol. Biol. 16, 678–680.

Ventura, A., Meissner, A., Dillon, C.P., McManus, M., Sharp, P.A., Van Parijs, L., Jaenisch, R., and Jacks, T. (2004). Cre-lox-regulated conditional RNA interference from transgenes. Proc. Natl. Acad. Sci. USA 101, 10380–10385.

Ventura, A., Kirsch, D.G., McLaughlin, M.E., Tuveson, D.A., Grimm, J., Lintault, L., Newman, J., Reczek, E.E., Weissleder, R., and Jacks, T. (2007). Restoration of p53 function leads to tumour regression in vivo. Nature 445, 661–665.

Viale, A., Pettazzoni, P., Lyssiotis, C.A., Ying, H., Sánchez, N., Marchesini, M., Carugo, A., Green, T., Seth, S., Giuliani, V., et al. (2014). Oncogene ablation-resistant pancreatic cancer cells depend on mitochondrial function. Nature 514, 628–632.

Von Hoff, D.D., Ervin, T., Arena, F.P., Chiorean, E.G., Infante, J., Moore, M., Seay, T., Tjulandin, S.A., Ma, W.W., Saleh, M.N., et al. (2013). Increased survival in pancreatic cancer with nab-paclitaxel plus gemcitabine. N. Engl. J. Med. 369, 1691–1703.

Waddell, N., Pajic, M., Patch, A.M., Chang, D.K., Kassahn, K.S., Bailey, P., Johns, A.L., Miller, D., Nones, K., Quek, K., et al.; Australian Pancreatic Cancer Genome Initiative (2015). Whole genomes redefine the mutational landscape of pancreatic cancer. Nature 518, 495–501.

Wang, P., Lin, C., Smith, E.R., Guo, H., Sanderson, B.W., Wu, M., Gogol, M., Alexander, T., Seidel, C., Wiedemann, L.M., et al. (2009). Global analysis of H3K4 methylation defines MLL family member targets and points to a role for MLL1-mediated H3K4 methylation in the regulation of transcriptional initiation by RNA polymerase II. Mol. Cell. Biol. 29, 6074–6085.

Ying, H., Kimmelman, A.C., Lyssiotis, C.A., Hua, S., Chu, G.C., Fletcher-Sananikone, E., Locasale, J.W., Son, J., Zhang, H., Coloff, J.L., et al. (2012). Oncogenic Kras maintains pancreatic tumors through regulation of anabolic glucose metabolism. Cell 149, 656–670.

Yu, B.D., Hess, J.L., Horning, S.E., Brown, G.A., and Korsmeyer, S.J. (1995). Altered Hox expression and segmental identity in Mll-mutant mice. Nature 378, 505–508.

Zender, L., Xue, W., Zuber, J., Semighini, C.P., Krasnitz, A., Ma, B., Zender, P., Kubicka, S., Luk, J.M., Schirmacher, P., et al. (2008). An oncogenomics-based in vivo RNAi screen identifies tumor suppressors in liver cancer. Cell 135, 852–864.

Zhou, B.B., Zhang, H., Damelin, M., Geles, K.G., Grindley, J.C., and Dirks, P.B. (2009). Tumour-initiating cells: challenges and opportunities for anticancer drug discovery. Nat. Rev. Drug Discov. 8, 806–823.